Intranuclear HSV-1 DNA ejection induces major mechanical transformations suggesting mechanoprotection of nucleus integrity

Alex Evilevitch[a,1] and Sophia V. Hohlbauch[b]

[a]Department of Experimental Medical Science, Lund University, Lund 22184, Sweden; and [b]Asylum Research, an Oxford Instruments Company, Santa Barbara, CA 93117

Edited by Ivet Bahar, Department of Computational and Systems Biology, University of Pittsburgh School of Medicine, Pittsburgh, PA; received July 30, 2021; accepted January 4, 2022

Maintaining nuclear integrity is essential to cell survival when exposed to mechanical stress. Herpesviruses, like most DNA and some RNA viruses, put strain on the nuclear envelope as hundreds of viral DNA genomes replicate and viral capsids assemble. It remained unknown, however, how nuclear mechanics is affected at the initial stage of herpesvirus infection—immediately after viral genomes are ejected into the nuclear space—and how nucleus integrity is maintained despite an increased strain on the nuclear envelope. With an atomic force microscopy force volume mapping approach on cell-free reconstituted nuclei with docked herpes simplex type 1 (HSV-1) capsids, we explored the mechanical response of the nuclear lamina and the chromatin to intranuclear HSV-1 DNA ejection into an intact nucleus. We discovered that chromatin stiffness, measured as Young's modulus, is increased by ∼14 times, while nuclear lamina underwent softening. Those transformations could be associated with a mechanism of mechanoprotection of nucleus integrity facilitating HSV-1 viral genome replication. Indeed, stiffening of chromatin, which is tethered to the lamina meshwork, helps to maintain nuclear morphology. At the same time, increased lamina elasticity, reflected by nucleus softening, acts as a "shock absorber," dissipating the internal mechanical stress on the nuclear membrane (located on top of the lamina wall) and preventing its rupture.

nucleus mechanics | DNA ejection | herpesvirus | atomic force microscopy | capsid

Mechanosensory mechanisms in cells regulate many cellular functions, including transcription factors, homeostasis, tumorigenesis, and cell fate "decisions" during viral infection (e.g., lytic or latent course of infection; Refs. 1–4). The primary cellular components that mediate mechanical homeostasis between cells and their environment are the cytoskeleton, including the actin and microtubule network, the integrin-based focal adhesions, and the nucleus (1). The focal adhesion–cytoskeleton–nucleus complex forms one integrated mechanical system that defines the cell's mechanosensory system, allowing it to respond to mechanical perturbations. Viral infection shifts homeostasis and leads to mechanical transformations within the cell that either maintain or disrupt nuclear integrity, which alters the cell's ability to replicate viral genomes (5–7). In this work, we explore how nucleus mechanics is impacted by intranuclear DNA ejection (without viral DNA replication) from human herpes simplex virus type 1 (HSV-1) in the course of herpesvirus infection. We use atomic force microscopy (AFM) force volume mapping to directly probe stiffness (measured as Young's modulus; Refs. 8, 9) of cell-free reconstituted nuclei incubated with HSV-1 capsids, which dock at the nuclear pore complexes (NPCs) and eject their DNA into the nucleus (10, 11). This isolated nucleus system recapitulates capsid–nucleus binding and viral DNA ejection (without DNA replication) in vivo without interference from trafficking kinetics of capsids moving toward the nucleus (12) while allowing direct probing of nucleus mechanics with the AFM cantilever. Previously, nucleus mechanics was investigated with AFM studies in intact cells (13). Investigating nuclear mechanics in intact cells complicates data interpretation since the nuclear mechanical response is obstructed by the cell membrane and cytoskeleton mechanics (cytoskeleton-mediated tension, in which focal adhesion-anchored actin cables pull down the nucleus, thereby partly compressing it) as well as by movement of the nucleus inside the cell (13). Furthermore, we optimized the number of capsids bound to each isolated nucleus to that of a lytically infected cell (100 to 200 capsids per nucleus); see justification of this parameter choice explained in *Reconstituted Virus–Nucleus System*. The typical HSV-1 burst size is 100 to 1,000 virions per infected cell (14–16). Also, the infectious virus/host cell ratio during HSV-1 reactivation from latency in e.g., TG (trigeminal ganglia) neuronal cells in vivo occurs at high multiplicity of infection (MOI) (15, 17–19).

For most DNA viruses and some RNA viruses, viral replication and assembly occur in the nucleus, where the nuclear membrane controls penetration of viral genome into the host, as well as the egress of mature virions (1, 20–22). The nucleus is separated from the cytoplasm by the double-membraned nuclear envelope and the nuclear lamina, which underlies the nuclear envelope; the nuclear lamina is composed of a meshwork of

Significance

We discovered major mechanical transformations in both chromatin and nuclear lamina at the initial stage of herpesvirus replication. We found that chromatin stiffness is dramatically increased, while nuclear laminar rigidity is decreased, immediately after viruses eject their genomes into a host cell nucleus. A stiffness increase in chromatin mechanics suggests a viral DNA–induced chromatin compaction, helping to maintain nuclear morphology. The observed softening of the nuclear lamina, on the other hand, provides mechanoprotection of the nuclear envelope since lamina act as an internal shock absorber for mechanical deformations. These transitions lead to a robust mechanical response aimed at maintaining nuclear integrity; this mechanism could facilitate viral genome replication. This is an observation of mechanoadaptation in cells utilized by herpesviruses.

Author contributions: A.E. designed research; A.E. performed research; A.E. and S.V.H. contributed new reagents/analytic tools; A.E. and S.V.H. analyzed data; and A.E. wrote the paper.

Competing interest statement: S.V.H. is employed at Asylum Research, Oxford Instruments, Santa Barbara, CA 93117.

This article is a PNAS Direct Submission.

[1]To whom correspondence may be addressed. Email: Alex.Evilevitch@med.lu.se.

This article contains supporting information online at http://www.pnas.org/lookup/suppl/doi:10.1073/pnas.2114121119/-/DCSupplemental.

Published February 23, 2022.

filament proteins called lamins functioning as a structural and mechanical scaffold for the nucleus (23). Chromatin is tethered to the nuclear lamina by specific proteins (24). The nucleus is the stiffest organelle in the cell; its mechanics is defined by the nuclear lamina and chromatin (1, 13, 25, 26). Mechanical strain on the nuclear envelope, in cancer cells, for example, can lead to nuclear rupture and subsequent DNA damage (27). Strain on the nuclear envelope is also increased during herpesvirus replication. The hundreds of viral DNA genomes and newly assembled viral capsids being synthesized in the nucleus gradually displace the nuclear chromatin until viral genome occupies most of the nuclear space (28), leading to increased strain on the nuclear lamina wall. This results in phosphorylation of lamina and lamina reorganization, which leads to disassembly or rupture of the nuclear envelope, facilitating virion egress (29). Thus, it is critical for infecting herpesvirus to maintain nucleus integrity to sustain its genome replication and maximize its progeny. It remains unknown, however, how the initial step of viral genome replication in the nucleus, namely intranuclear viral genome ejection, affects nucleus mechanics.

We found a striking mechanical transformation occurring in the stiffness of both nuclear chromatin and lamina in response to HSV-1 DNA ejection—chromatin stiffness is dramatically increased by ∼14 times, while the stiffness of nuclear lamina is decreased. The dramatic increase in the chromatin stiffness immediately after viral DNA ejection suggests increased chromatin compaction, which could be induced by nonrandom interactions between herpesvirus genomes and chromatin regions, leading to histone rearrangement (30). Higher chromatin rigidity has been shown to protect the nucleus from mechanical force deformations by preserving nucleus morphology, as chromatin is tethered to the lamina (31). At the same time, softening of nuclear lamina has been previously discovered in the context of functional demands and longevity of human skin epidermis stem/progenitor cells (EPCs) that require efficient mechanisms to counteract nuclear DNA damage from mechanical deformation (7). The mechanism of lamina softening allows EPCs to restore their steady-state nuclear and chromatin architecture for long-term mechanoprotection (7). We observe a similar mechanical softening transformation in the nuclear lamina induced by intranuclear viral genome ejection. This finding helps to explain how herpesvirus genomes penetrate the nucleus while avoiding nucleus damage: by dissipating the mechanical stress on the nuclear membrane through nuclear lamina softening, acting as a "shock absorber." To support viral fitness, viruses have utilized various mechanisms to maintain the integrity and functionality of the host cell required for viral replication (e.g., cyanophages even encode bacterial photosynthetic machinery to keep cyanobacteria alive during phage replication; Ref. 32). Our discovery demonstrates another paradigm of virus–host interaction, in which nuclear mechanics is modulated by the infecting herpesviruses to enable the nucleus to withstand the mechanical stresses induced by viral genome internalization, preventing premature damage of the nuclear DNA replication machinery, which is exploited by the virus.

This work is divided into four sections. In *Reconstituted Virus–Nucleus System*, we describe the design of the isolated HSV-1 virus–nucleus system as well as the controls used to differentiate changes in nucleus mechanics in response to capsid attachment to NPCs alone (which affects NPC permeability and therefore nucleus mechanics) and in response to viral DNA ejection into a nucleus following capsid attachment. In *Topographical Imaging of HSV-1–Infected Nuclei*, we demonstrate that this reconstituted nucleus system permits high-resolution AFM imaging of HSV-1 capsids attached to the NPCs and offers the capability to conduct direct AFM mechanical mapping of infected nuclei. Next, we perform AFM force volume mapping of nuclei without and with HSV-1 capsids docked at the NPCs (resulting in viral DNA ejection) and determine stiffness response of the nuclear chromatin [without glutaraldehyde (GA) fixation; *Mechanical Response of the Nuclear Chromatin to HSV-1 DNA Ejection*] and separately of the nuclear lamina (with GA fixation of the lamina meshwork; *Mechanical Response of the Nuclear Lamina to HSV-1 DNA Ejection*).

Results and Discussion

Herpesviruses present an intriguing nanomechanical system. They package their micrometer-long double-stranded DNA (125 to 230 kbp long, depending on the type of herpesvirus) into a nanometer-scale spherical icosahedral capsid with the help of a viral ATPase motor, located at one unique capsid vertex. We found that the packaging process creates tens of atmospheres of mechanical pressure on the capsid interior because of the tight packaging of negatively charged DNA in a rigid protein capsid (33). The DNA-filled herpesvirus capsid is surrounded by an unstructured protein layer, the tegument, and a lipid envelope. Over the course of infection, after binding at the outer host cell membrane, viruses enter the cell cytoplasm, are transported toward the nucleus, and dock to the NPC, which forms a passageway for molecular traffic into the nucleus; the viral capsid then ejects its genome (34). HSV-1 genome pressure is responsible for DNA ejection into a host cell nucleus (10). As mentioned above, during HSV-1 reactivation from latency in TG neurons at high MOI (17–19), tens of HSV-1 virus capsids simultaneously adsorb to NPCs on a single cell nucleus and eject viral genomes (10, 11). [This process is repeated as empty capsids detach and new DNA-loaded capsids are docked at the NPCs in vivo (35).] A single round of HSV-1 DNA ejections leads to internalization of millions of base pairs of viral DNAs in the nucleus; HSV-1 DNA quickly decondenses once in the nucleus, occupying three times more volume than in the capsid (36). The ejected DNA accumulates initially underneath the nuclear lamina surface in close proximity to the NPC injection sites (36). This suggests that nuclear lamina is under strain from ejected herpesvirus genomes, even before viral genome replication takes place. We investigate here the effect of this viral DNA–induced lamina strain on nuclear mechanics.

Furthermore, as mentioned above, nuclear chromatin also plays a major role in the nucleus' response to mechanical deformation (25). Chromatin and its compaction level, modulated by histone–DNA interactions (30), provide rigidity and stabilize nucleus morphology, protecting the DNA (25). Alterations in chromatin compaction (e.g., caused by disease) correlate with its mechanical response to deformation and can lead to loss of nuclear shape and stability (31), causing nuclear rupture and DNA damage. Thus, chromatin-controlled nuclear stability provides a mechanism of mechanoprotection of nucleus functionality (31). However, viral DNA ejected into the nucleus from tens of HSV-1 capsids (during one round of viral DNA ejection events from capsids docked simultaneously at NPCs) only adds several million base pairs to the nucleus, increasing nucleotide amount by less than 1% (chromosomal DNA has on average three billion base pairs of nucleotides; Ref. 37). This raises a central question: Does this small change in the nucleic acid amount in the nucleus after herpesvirus DNA ejection but prior to viral genome replication affect nuclear stability through interactions between viral genomes and chromatin, affecting chromatin compaction (30)?

The nuclear mechanical response at small AFM tip indentations (in comparison to nucleus size) is dominated by chromatin stiffness since lamina forms a flexible meshwork with lower rigidity than chromatin (25, 38). Thus, by collecting AFM force volume maps on the nuclear surface without and with HSV-1 capsids docked at NPCs, we reveal the mechanical response of the nuclear chromatin. Separately, we also determine the

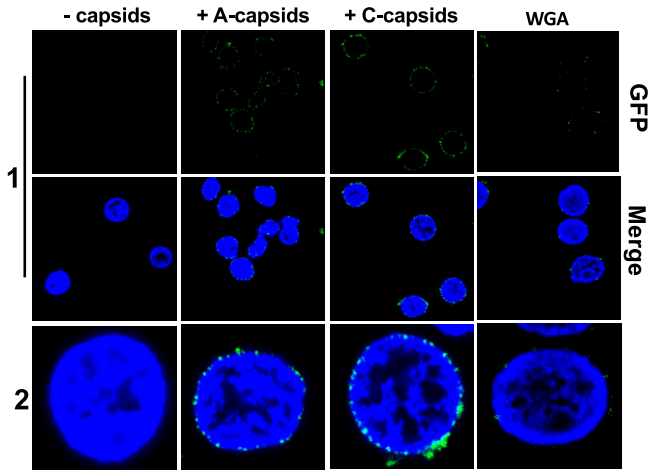

Fig. 1. Imaging of a reconstituted capsid–nuclei system confirms specific binding of A- and C-capsids to the NPCs at the nuclear membrane. Confocal fluorescence microscopy images show binding of GFP-HSV-1 A- and C-capsids (green) to DAPI-stained isolated nuclei (blue), in the presence of cytosol and ATP-regeneration system. The addition of WGA decreases capsid binding to nuclei for both capsid types, which demonstrates that capsids bind specifically to NPCs as opposed to binding anywhere on the nuclear membrane. The images at the bottom of row two are a zoom-in of the individual nuclei.

nuclear lamina's mechanical response to AFM indentation by decoupling the mechanical response of chromatin stiffness from nuclear lamina mechanics through chemical cross-linking of the lamina meshwork with GA, which does not cross-link nucleic acids (39, 40). Thus, GA fixation increases lamina shell rigidity above that of chromatin rigidity, making the contribution of chromatin stiffness to the overall nucleus mechanics negligible (this approach is explained in more detail in *Mechanical Response of the Nuclear Lamina to HSV-1 DNA Ejection*). GA fixation was done after the incubation of capsids with nuclei, allowing viral DNA ejection to occur. We analyzed with AFM force volume mapping the comparative change in the stiffness of the nuclear lamina (captured with GA fixation) prior to and after viral DNA ejection (nuclei without HSV-1 capsids and nuclei after incubation with HSV-1 capsids, respectively).

Reconstituted Virus–Nucleus System. We probe nucleus mechanics directly through AFM force volume mapping of a reconstituted capsid–nuclei system. This experimental setup builds on the previous observation that HSV-1 capsids bind specifically to NPCs of isolated rat liver cell nuclei reconstituted in cytosol and supplemented with an ATP-regeneration system (*Materials and Methods*) (11). Using a pull-down assay combined with qPCR, we showed earlier that HSV-1 capsid–NPC binding in isolated reconstituted nuclei triggers the ejection of viral DNA and its internalization in the nucleus, driven by capsid DNA pressure of ∼18 atm (10). A benefit of the reconstituted virus–nucleus system is that it can be used to isolate the effect of the central step of viral infection—capsid docking at the nucleus and viral genome uncoating—on nucleus mechanics while avoiding interference from other processes occurring within the cell cytoplasm during viral replication (12). There are, on average, more than a thousand NPCs covering a significant area of the nucleus surface (41). Viruses binding to NPCs attach to nucleoporins (Nups) within the NPC structure and modulate NPC permeability (20). Increased permeability of the nuclear envelope is expected to affect its viscoelastic modulus. Therefore, the stiffness of an infected cell nucleus is expected to be modulated by both attachment of capsids to NPCs (where attached capsids cover a significant fraction of the nuclear surface resulting in increased nucleus permeability) and separately by viral DNA ejection from capsids into the nucleus. To separate these two contributions to the AFM-measured nucleus mechanical response, it is essential to set up a control experiment consisting of empty capsids (incapable of DNA ejection) docked at the NPCs. The HSV-1 capsid assembly process offers a unique opportunity to accomplish this because capsid assembly intermediates that consist of stably copurified DNA-filled capsids (C-capsids) and empty capsids (A-capsids) can be isolated (42–44). A- and C-capsids contain the same number of major capsid proteins, portal forming protein (UL6), and triplexes; they are essentially structurally identical, and therefore, their mechanical properties can be directly compared using the AFM approach (45). Thus, quantification of nucleus stiffness with attached DNA-filled C-capsids and empty A-capsids provides reference points for nucleus stiffness measurements before and after viral DNA ejection, respectively. However, the feasibility of this control must first be confirmed by demonstrating that A-capsids can bind to NPCs similarly to C-capsids. To verify A-capsid binding efficiency to NPCs, purified A-capsids were added to isolated cell nuclei from rat liver cells (at the same concentration as C-capsids), supplemented with cytosol and ATP-regeneration system, and incubated at 37 °C. Fig. 1 shows confocal fluorescence microscopy and Fig. 2 shows super-resolution structured illumination microscopy (SR-SIM) images of green fluorescent protein (GFP)-labeled HSV-1 A- and C-capsids, respectively (green, strain K26GFP, HSV-1 strain expressing GFP-tagged VP26 protein), at the surface of DAPI-stained cell nuclei (blue). SR-SIM provides resolutions down to 120 nm, allowing visualization of individual capsids attached to the nucleus. We found that A-capsids bind to the NPCs at similar levels as C-capsids. As a negative control, we used wheat germ agglutinin (WGA), which at high amounts (0.1 to 0.5 mg/mL) associates with the glycoproteins within the NPC with high affinity (11, 46, 47) and decreases capsid binding, demonstrating capsid–NPC binding specificity (as opposed to random binding to the nuclear membrane); see Fig. 1. As a complementary approach, we also visualized capsid binding to NPCs by ultrathin-sectioning electron microscopy (EM), which further confirmed docking of capsids to the NPCs. Fig. 2 shows EM micrographs of A- and C-capsids bound to the NPC basket

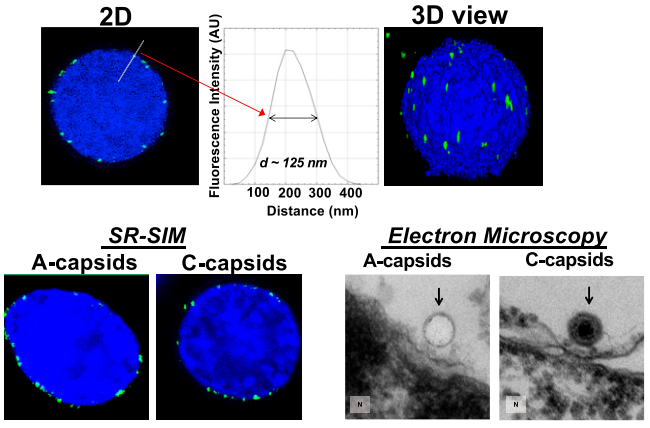

Fig. 2. Representative SR-SIM images show GFP-HSV-1 A- and C-capsids (green) bound to isolated rat liver nuclei (blue DAPI stain) with similar nuclear surface occupancy. As a complementary approach, we also visualized capsid binding to NPCs by ultrathin-sectioning EM, which further confirmed docking of capsids to the NPCs. Figure shows EM micrographs of A- and C-capsids bound to the NPC basket on a nucleus surface (the observed density inside the C-capsids corresponds to packaged DNA before it is ejected into the nucleus since sample was kept at 4 °C prior to fixation, while DNA ejection occurs at 37 °C; Ref. 10).

on a nucleus surface (the observed density inside the C-capsids corresponds to packaged DNA before it is ejected into the nucleus since the sample was kept at 4 °C prior to fixation, while DNA ejection occurs at 37 °C; Ref. 10). Thus, the ability to bind empty A-capsids to isolated nuclei allows us to separate the effect of capsid–NPC binding on nucleus mechanics without interference from viral DNA ejection into the nucleus.

As mentioned above, the virus capsid/nucleus ratio used for AFM measurements was optimized to correspond to the physiologically relevant ∼100 to 200 capsids docked at the nucleus surface. HSV-1 can initiate a productive infection cycle under extremely low MOI (essentially one genome per infected cell). However, each cell will produce thousands of virions that will infect surrounding cells at a high MOI (MOI > 50) (15). It is important to stress the difference between the definition of MOI and the number of HSV-1 capsids attached per nucleus. MOI is defined as the "number of infectious virions"/"number of cells." In the case of HSV-1, the number of infectious viruses is usually determined by measuring the virus concentration that is added to a cell culture using plaque assay and is therefore provided by PFUs (plaque-forming units). This implies that viruses can complete the replication cycle and lyse the cell. However, not all capsids docked at the nucleus are capable of completing a viral replication cycle. Hence, for herpes simplex viruses, the viral particle/PFU ratio is 50 to 200 (depending on the infected cell type) (48). Indeed, even at lower MOI values (1, 10) in GFP/HSV-1–infected Vero cells, we observed ∼100 to 200 capsids docked at a nucleus accumulated over time [3 to 4 h postinfection (hpi)] as capsids that enter the cell are being actively transported toward the nucleus along the microtubular network (Fig. 3 *A* and *B* show infection at MOI = 10). In order to confirm the number of bound capsids per nucleus, we collected 3D stack images of nuclei with attached capsids using confocal fluorescence microscopy for GFP/HSV-1 capsids bound to DAPI-stained nuclei; see Fig. 3. We used Z-projection (2D) of the 3D stack to quantify individual capsids, using ImageJ software automation, averaging over at least 50 nuclei (and thousands of capsids) for each sample (*Materials and Methods*). Fig. 3*D* shows the histogram distribution of C-capsids/isolated nucleus with a mean value of ∼170. We previously showed using ultrathin-sectioning EM that ∼77% of C-capsids bound to an isolated nucleus eject their DNA (49). Thus, on average, ∼130 HSV-1 genomes are released into each nucleus. As mentioned above for direct comparison, we quantified the number of capsids at the nucleus surface in wild type (wt) GFP/HSV-1–infected Vero cells at MOI = 10; see Fig. 3 *A* and *B* (cell nuclei were stained with DAPI). Fig. 3*A* shows the progression of HSV-1 replication versus hpi. We determined that at 3.5 hpi, the maximum capsid number at the nucleus membrane in a cell is reached before new virus assembly occurs in the nucleus. Using the same confocal fluorescent imaging approach (3D stack to Z-projection conversion) for quantification of capsids at the nucleus, we found an average of ∼160 capsids/infected cell nucleus at 3.5 hpi (see histogram in Fig. 3*D* collected for at least 50 nuclei), corresponding to the number of capsids bound to an isolated reconstituted nucleus. It is not likely to be a coincidence that we observed ∼100 to 200 capsids attached per nucleus in both infected Vero cells and isolated nuclei. It is important to note that for isolated nuclei, we added capsids in excess, reaching the saturation of the nucleus's capsid-binding capacity. This suggests that even at lower MOIs, after a sufficiently long postinfection time, the number of capsids docked per nucleus is limited by the number of available NPCs on the nucleus surface as well as nucleus geometry, rather than the MOI value. Indeed, saturated genome entry into a nucleus has been independently observed during lytic replication of HSV-1 (15).

In *Topographical Imaging of HSV-1–Infected Nuclei*, we demonstrate the feasibility of AFM 3D topographical imaging of virus–nucleus interaction. Confirming with AFM that individual capsids and NPCs can be resolved on the nucleus surface will facilitate AFM force volume mapping experiments of the capsid–nucleus surface mechanics in *Mechanical Response of the Nuclear Chromatin to HSV-1 DNA Ejection* and *Mechanical Response of the Nuclear Lamina to HSV-1 DNA Ejection*.

Topographical Imaging of HSV-1–Infected Nuclei. Neither AFM topographical imaging of viruses docked at the intact nucleus nor direct recording of the nuclear mechanical response to a viral infection have been demonstrated. In the previous AFM imaging studies of HSV-1 capsids on the nuclear surface, the nuclear membrane was isolated (the chromatin was removed), fixed with GA, and spread on an AFM slide surface in order to image structural details of virus attachment on a 2D membrane (50). In this work, we show that isolated and reconstituted intact nuclei with HSV-1 capsids adsorbed at NPCs provide a robust experimental system for both AFM structural analysis and interrogation of mechanical transformations associated with the central step of viral infection: viral capsid binding at the nuclear membrane followed by viral genome ejection into the nucleus.

We used Fast Force Mapping mode (FFM mode on Cypher ES AFM, Oxford Instruments Asylum Research; *Materials and Methods*) to resolve high-resolution structures of delicate viral capsids on the nucleus surface because of the improved force control between the tip and sample, the ability to use very low (piconewton) applied force, and an increase in sample stiffness with higher indentation velocity. A challenge presented by AFM imaging of individual viral capsids on an intact apical nucleus surface is the fact that the nuclear envelope is expected to have a softer mechanical response than the capsid (45). This suggests that capsids would be pushed into the nucleus surface, resulting in nucleus surface probing rather than capsid surface probing (a general AFM imaging requirement is to place a soft object on a hard substrate surface) (51). However, as with most biomaterials, nuclei and capsids display viscoelastic behavior, in which apparent stiffness depends on indentation velocity. Indeed, we have found that nucleus stiffness strongly depends on the indentation velocity of the AFM cantilever (*SI Appendix*, Fig. 1). Nucleus stiffness is increased with increased tapping velocity since the nucleoplasm approaches the response of an incompressible medium at higher indentation velocity (26, 52). At the same time, HSV-1 capsids show a predominantly elastic response even at high AFM indentation velocity and therefore do not exhibit strong dependence on the AFM tapping velocity (53). Thus, high AFM probing frequency of the capsid–nucleus surface (we choose 500 Hz in FFM mode) stabilizes the nucleus surface, acting as substrate for attached HSV-1 capsids. This further improves FFM imaging resolution. Alternating AFM tip tapping velocity is a common approach used in AFM microrheology of cells, in which modulation of tapping velocity helps to display different nanostructures on the cell surface due to differences in viscoelastic (dynamic Young's modulus value) and elastic (constant Young's modulus value) behavior of cellular components (52, 54, 55).

For topographical imaging of capsid attachment to NPCs at the nuclear membrane, purified HSV-1 capsids were incubated with isolated nuclei supplemented with cytosol and ATP-regeneration system. After incubation, the sample was fixated with 2% GA, washed, and resuspended in capsid-binding buffer (CBB), after which it was deposited on hydrophobically modified AFM slides for imaging (*Materials and Methods*). Fixation of the nuclei in GA cross-links the lamina meshwork (39, 40), which increases nucleus surface stiffness by ∼10 times (as shown below). Since fixation provides increased nuclear surface rigidity, it significantly improves the imaging resolution of capsids on the nuclear surface. (Fixation of the sample, however, is not required for the determination of nucleus chromatin

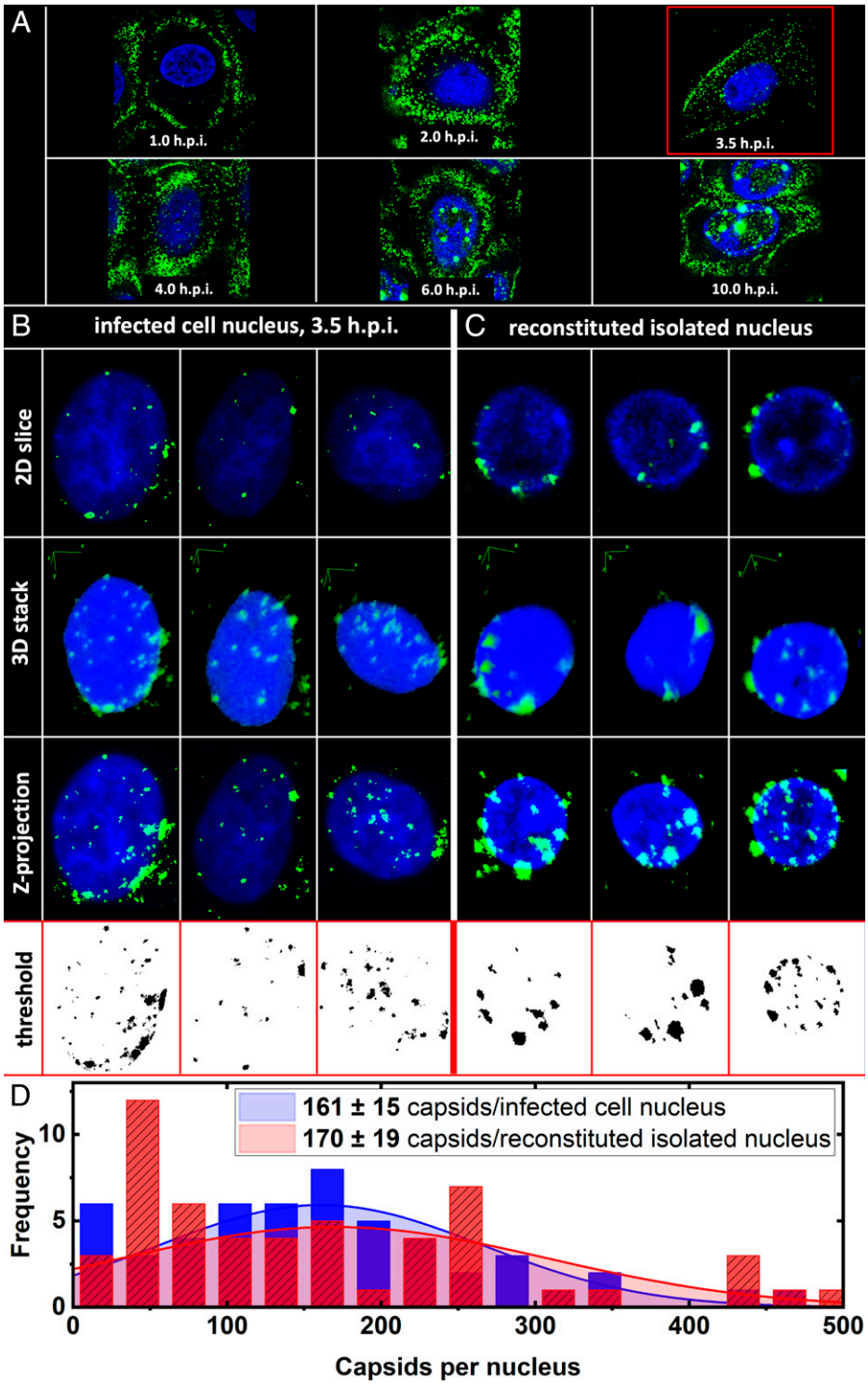

Fig. 3. Quantification of capsids docked at the nuclear membrane. (*A*) Infection progression of GFP/HSV-1–infected Vero cells. At 3.5 hpi, the maximum number of capsids is reached before new capsids are assembled in the nucleus. (*B*) Steps of confocal fluorescence image analysis are shown for quantification of capsids per nucleus in infected Vero cells at 3.5 hpi. (*C*) Steps of confocal fluorescence image analysis are shown for quantification of capsids per isolated cell nucleus. First row is a 2D slice (one focal plane) from the 3D stack GFP capsids (green) on DAPI-stained nucleus (blue) in the second row. Next row is a Z-projection in 2D of all confocal plane slices in the 3D stack that was used for quantification of individual capsids, built using nonoverlapping green pixels with the highest intensity from each slice (corresponding to capsids). Z-projection shows both channels and exhibits the projection of all capsids on a nucleus. The green channel was converted to a binary image using a threshold, as shown in the last row, in order to accurately compute number of capsids bound at each nucleus. Capsids outside of the nuclear membrane surface are not counted (as seen in the threshold images). Some nuclei showed capsid aggregates at the surface. The number of capsids in each aggregate was quantified using number of pixels corresponding to an individual capsid applied only to the aggregate surface area immediately at the nuclear membrane, independent of the height of the aggregate. Automated capsid counting using these boundary conditions was performed with ImageJ software script. (*D*) Histograms showing the distribution of the computed number of capsids docked at the membrane of an infected cell nucleus and a reconstituted isolated nucleus, respectively. At least 50 nuclei were quantified for each sample.

mechanics, as shown in *Mechanical Response of the Nuclear Chromatin to HSV-1 DNA Ejection*.) Prior to AFM imaging, nuclei were located optically with the built-in TopView optics (Fig. 4 *A* and *B*). Fig. 4*B* shows an AFM imaged area of the nucleus surface overlayed on top of the optical image of a nucleus. First, we imaged with AFM the topographic surface of the isolated nucleus without viral capsids in CBB (*Materials and Methods*). As the next sample, nuclei were incubated with HSV-1 capsids at 37 °C for 40 min and washed in CBB. Liquid sample was deposited on the AFM substrate for imaging. Fig. 4 *C–F* show representative 3D topography AFM images of the nuclear membrane surface with well-resolved HSV-1 A-capsids docked at the NPC baskets (similar images were obtained for C-capsids). The nucleus surface of rat liver cells is densely covered with protruding NPC baskets, providing binding sites for HSV-1 capsids (Fig. 4*C*). Capsids on the nucleus surface are displaying faceted icosahedral features as well as resolved individual capsomer subunits characteristic of the HSV-1 capsid structure. The capsid height measured on top of the nuclear membrane surface is ~124 nm, which is in agreement with a cryo-EM–obtained

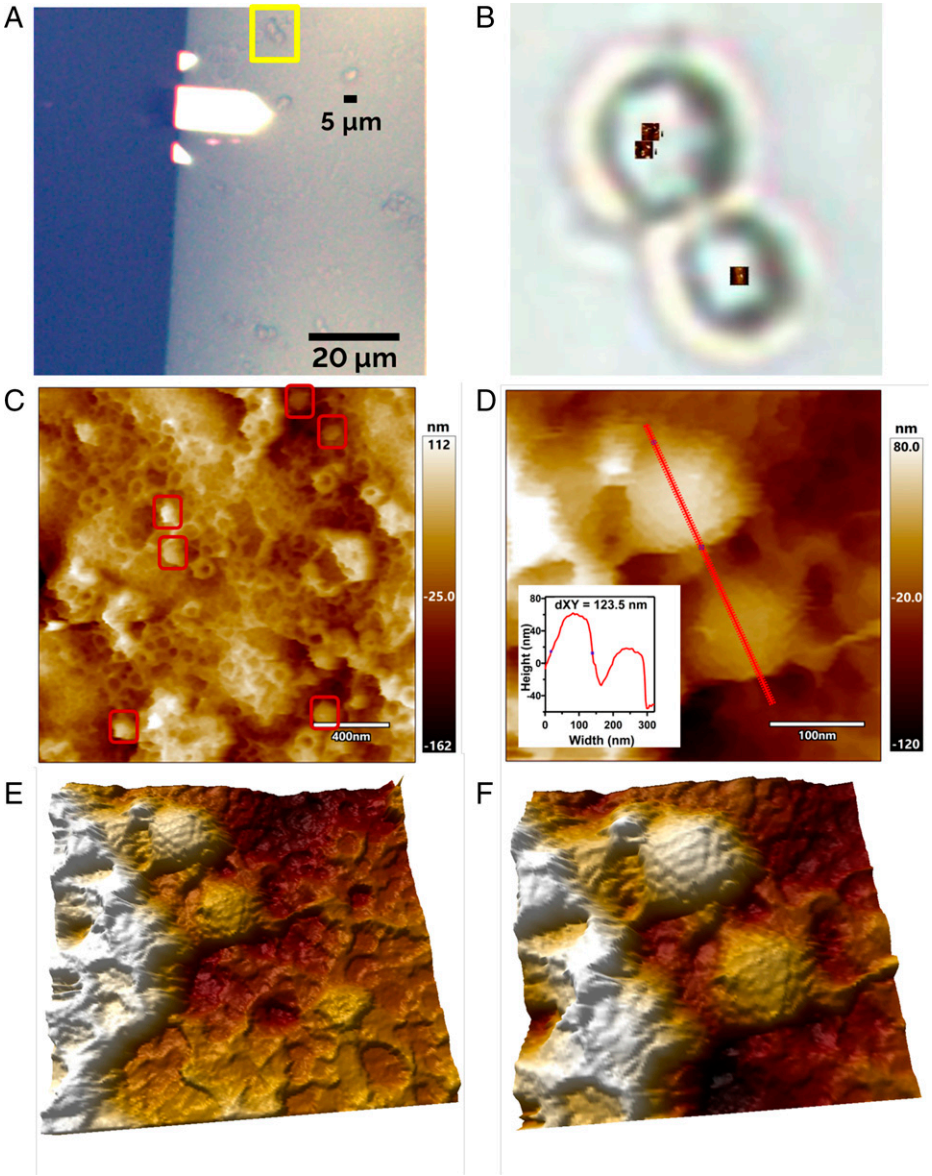

Fig. 4. A panel showing AFM FFM imaging sequence. (*A*) Zoomed-out top view optical image and (*B*) zoomed-in optical image before moving the cantilever above the nucleus. (*C*–*F*) A representative 3D topography AFM image of the nuclear membrane surface with well-resolved NPC baskets with HSV-1 A-capsids attached (similar images were obtained for C-capsids). Capsids were incubated with nuclei at 37 °C for 40 min in cytosol and ATP regeneration system. After incubation, nuclei were fixated with 2% GA, increasing nuclear envelope rigidity and improving AFM imaging resolution, and washed in CBB for imaging. AFM image shows that the nucleus surface of rat liver cells is densely covered with protruding NPC baskets, providing binding sites for HSV-1 capsids. Capsids on the nucleus surface are displaying faceted icosahedral features as well as resolved individual capsomer subunits characteristic of HSV-1 capsid structure. The capsid height measured on top of the nuclear membrane surface is ∼124 nm, which is in agreement with a cryo-EM–obtained value of 125 nm for HSV-1 capsid diameter (56).

value of 125 nm for HSV-1 capsid diameter (56). Our previous data with AFM topography of purified HSV-1 capsids alone in buffer solution on a hydrophobic glass surface showed analogous capsid features (45). This demonstrates that the reconstituted capsid–nucleus system is suitable for AFM structural analysis and, therefore, can be used for characterization of nucleus mechanical response to AFM force volume mapping before and after viral DNA ejection.

Mechanical Response of the Nuclear Chromatin to HSV-1 DNA Ejection. A nucleus' mechanical response is dominated by chromatin (where the state of DNA condensation is reflected by the nucleus stiffness) and nuclear lamina (primarily by lamin isoforms A and C forming layers under the nuclear membrane and providing nucleus rigidity) (13, 25, 57). Chromatin is tethered to the lamina through various proteins. In the previous nucleus mechanics studies performed on intact cells (13, 57), strain in nucleus volume was found to occur at small AFM indentations (<3 µm, where average nucleus diameter is ∼5 to 6 µm), where nucleus stiffness response to external deformation is controlled predominantly by the chromatin (25). At the same time, the strain in the nucleus area occurs at large AFM indentations (over 50% deformation of nucleus height), where stiffness response to external deformation is controlled by A/C-type lamins. In this section, we performed AFM force volume mapping at small indentations of nucleus surface relative to its dimension to probe the mechanical response of nuclear chromatin to viral DNA ejection from HSV-1 capsids docked at the nuclear membrane. Force volume map AFM analysis does not require high imaging resolution, and all samples were force volume mapped without fixation.

First, we performed our force volume mapping experiment on an unfixed nucleus surface in CBB without capsids, providing a reference point for stiffness of an uninfected nucleus. Then, we collected force volume maps for HSV-1 A-capsids and C-capsids, respectively, attached to nuclei in CBB; nuclei and capsids had been incubated for 40 min at 37 °C in cytosol and ATP-regeneration system (the incubation triggers DNA ejection from C-capsids into nucleus; Ref. 10). Force volume mapping uses lower AFM tip indentation velocity, ∼0.15 Hz (300 nm/s, which we determined to be the equilibrium indentation rate below which nucleus modulus does not change; *SI Appendix*, Fig. 1), in comparison to 500 Hz in FFM mode. A 10 × 10 force volume map (corresponding to 100 force–distance curves) was acquired over a 200 nm × 200 nm

area at the center of each nucleus, where the surface is typically the flattest. The nucleus indentation force was adjusted to achieve ∼300 nm of nucleus indentation (corresponding to small indentations in comparison to its size; Ref. 25). Fig. 5*A* shows a representative force volume map for unfixed nucleus without capsids. Several force volume maps were captured for each sample. Young's modulus of the nuclei (elastic modulus describing the amount of strain and reflecting the stiffness) was calculated by applying the Hertz contact mechanics model for a cone indenter to each force curve (*Materials and Methods*) (8, 9). Fig. 5*B* (red curve) shows a representative force–distance (Fz) curve, comprising each force volume map, for nucleus indentation with HSV-1 C-capsids attached. We observed that some Fz curves displayed a "notch" in the deformation behavior; see Fig. 5*B* (blue curve). The signature of a force curve can reveal information on the composition of the sample being indented. For example, if multiple slopes in the contact region are visible, then the material is most likely heterogenous, comprising different layers or regions with varying moduli (58, 59). This is typical for tissues, organs, or known complex multilayered material. When capsids are bound to the nuclear membrane, a similar complex system is created if the cantilever happens to be placed on top of a capsid that is attached to the nucleus. In this force curve, the cantilever first pushes into the capsid and then continues to indent into the nucleus. The observed drop in the Fz curve could reflect detachment or breaking of the capsid at the nucleus surface. When force indentation curves are acquired on nuclei without capsids, this notch is not detected. It can be noted that although a higher modulus is expected for the capsid (45), it is attached to a softer nucleus acting as a substrate, so the calculated apparent modulus of capsid indentation on top of a nucleus is an average, and more closely matches the modulus of the nuclei. Indeed, applying the Hertz contact mechanics model (gray line in Fig. 5*B*), we calculated the modulus of capsid and nucleus indentation by fitting the first Fz slope (corresponding to capsid indentation) before the notch with the fit range set to ∼10 to 55% of indention depth (z). To calculate the second slope, associated with the indentation into the nucleus, the fit range was set ∼10 to 85% of indention depth (z) and manually adjusted to follow the contour of the second slope, which was identical to the slope in the Fz curve without the notch (red curve). The calculated moduli for both slopes were essentially the same, but only the nucleus modulus is used for the data analysis immediately below.

Young's moduli for 100 Fz curves in each force volume map were repeatedly collected for several nuclei as well as on several areas of the same nucleus. All Young's moduli values were collectively plotted for each type of sample in a histogram for nuclei without capsids, nuclei with attached A-capsids, and nuclei with attached C-capsids (Fig. 6*A*). The Gaussian fit to the data in the histograms yields the average value and the SE. Measured average Young's moduli were E (nucleus without capsids) ∼49.6 ± 0.6 kPa, E (nucleus with A-capsids) ∼17.2 ± 0.2 kPa, and E (nucleus with C-capsids) ∼242.8 ± 3.2 kPa; see Fig. 6*A* and Table 1. First, we observed an ∼3-fold decrease in the nucleus stiffness when empty A-capsids are docked at the NPCs. Different virus families, which reproduce in the nucleus, employ various strategies for delivery of viral genome into cells (20). For example, the adenovirus capsid docks at the NPC and disassembles through Nup214 interaction, causing displacement of the Nups, resulting in increased permeability of the NPC (20). HSV-1 docking at the NPC is mediated by the minor capsid proteins, which also bind Nup214 situated on the cytoplasmic NPC surface (60, 61). The observation of a strong decrease in nucleus stiffness associated with binding of empty A-capsids at the NPCs suggests that HSV-1 binding also causes displacement of Nups, resulting in increased NPC permeability. This can be likened to "perforation" of the nuclear wall, leading to nucleus softening.

Next, we compared nucleus stiffness with docked empty A-capsids to nucleus stiffness with docked DNA-filled C-capsids. Nucleus stiffness was dramatically increased by ∼14 times for nucleus-bound C-capsids compared with bound A-capsids; see Fig. 6*A* and Table 1. The observed increase in nucleus stiffness could reflect an increased compaction of the nuclear chromatin triggered by its interaction with the herpesvirus genomes. As mentioned above, at small AFM indentations used in this study,

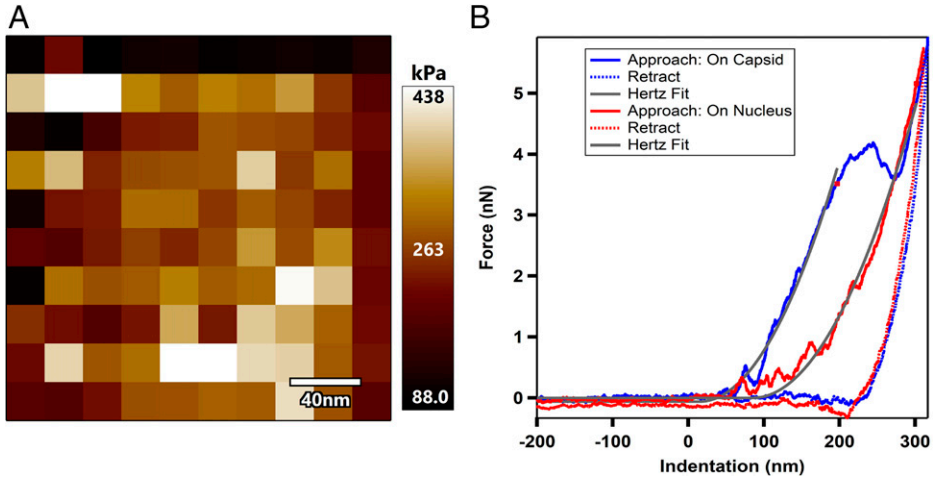

Fig. 5. (*A*) A representative 10 × 10 force volume map for unfixed nucleus with attached C-capsids (corresponding to 100 Fz curves) acquired over a 200 nm × 200 nm area at the center of each nucleus. (*B*) A representative Fz curve, selected from one of the acquired force volume maps: cantilever approach and indentation into C-capsid bound nucleus (solid red line). Some Fz curves displayed a "notch" in the deformation behavior (blue line). In this force curve, the cantilever first pushes into the capsid and then continues to indent into the nucleus. The observed drop in the Fz curve could reflect detachment or breaking of the capsid at the nucleus surface. When force indentation curves are acquired on nuclei without capsids, this notch is not detected. Force indentation curve acquired on a nucleus shows only one slope, which represents the response of the nucleus only. Moduli was calculated using the Hertz contact mechanics model. Contact point, depth, and force offsets were autoselected by the software. Fit range was adjusted as needed to maintain an indentation depth of 300 nm. Cantilever retraction (dashed red and blue lines) and fit using Hertz mechanics model for Young's modulus determination (solid gray line).

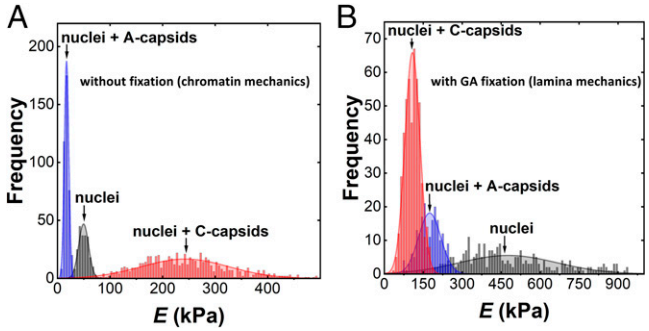

Fig. 6. Young's moduli for 100 Fz curves in each force volume map were repeatedly collected for several nuclei as well as for several areas on the same nucleus. All moduli values were collectively plotted for each type of sample in a histogram for nuclei without capsids, nuclei with attached A-capsids, and nuclei with attached C-capsids, respectively. (*A*) Histograms of Young's moduli for all samples without fixation, reflecting chromatin stiffness. (*B*) Histograms of Young's moduli for all samples with 2% GA fixation, reflecting relative nuclear lamina stiffness. The Gaussian fit to the data in the histograms yields the average value and the SE shown in Table 1.

chromatin is a major mechanical component of the nuclear stiffness response (25). It was previously shown that the state of chromatin compaction has a direct link to the nuclear curvature, which in turn affects the nuclear viscoelastic modulus measured by AFM (57). Viral genome ejection into the nucleus during infection has been shown to impact the structure of the host chromosome when it interacts with viral DNA (30). Host–viral genome interactions preferentially occur in specific regions of the host genome that are associated with open and early replicating chromatin, affecting its compaction. This leads to rearrangements in chromatin morphology by the tethered histones, affecting its compaction state and resulting in increased chromatin stiffness (62). (The locations of viral DNA in the host genome may be mechanistically linked to the epigenetic changes in the host genome upon viral infection; Ref. 30.) Recent chromatin-based nuclear mechanics studies suggest that increased nucleus rigidity provided by chromatin helps to maintain nuclear mechanical stability, protecting it from DNA damage (31). Weakened nuclear mechanics and abnormal morphology have been shown to cause rupturing of the nucleus, which results in nuclear dysfunction (31). Herpesviruses rely on nuclear integrity to preserve the nuclear DNA replication machinery required for viral replication. Since viral DNA and nuclear chromatin interactions are not random (30, 36), the observed increase in the nucleus stiffness at the initial stage of intranuclear herpesvirus DNA ejection could suggest a virus-controlled mechanism of nucleus stabilization, facilitating viral replication in intact nuclei. It is remarkable that while viral DNA ejected into a nucleus constitutes less than 1% of the nuclear chromatin nucleotide amount (37), it shows a profound effect on the chromatin stiffness, increasing it by an order of magnitude.

As noted above, immediately after DNA ejection, viral genomes remain in the proximity of the lamina inner wall surface (36), which leads to strain on the lamina. In *Mechanical Response of the Nuclear Lamina to HSV-1 DNA Ejection*, we investigate the mechanical response of nuclear lamina to herpesvirus DNA ejection by decoupling the mechanical response of lamina stiffness from the chromatin stiffness through chemical cross-linking of the lamina meshwork.

Mechanical Response of the Nuclear Lamina to HSV-1 DNA Ejection. As we discovered above, herpesvirus genome ejection into the nucleus leads to a dramatic stiffening of the nuclear chromatin, which helps to maintain nuclear morphology despite viral DNA ejection. However, viruses replicating in the nucleus also utilize nuclear lamina mechanics (regulating nuclear integrity) since lamina constitute a barrier for virions entering or escaping the nucleus (29). Lamins are critical for protection of nucleus integrity, helping to maintain the nuclear shape and participating in diverse nuclear processes including DNA replication (29). Thus, it is also central to investigate the effect of HSV-1 DNA ejection on lamina mechanics. Here, we ask a central question: Does the nuclear lamina adapt to mechanical strain induced by viral DNA ejection on the lamina meshwork?

The nuclear lamina forms a compressed network shell of interconnected lamin rods that is extensible but limited in compressibility from the native state. When subjected to large deformations (more than 50% of the nucleus height), lamin isoforms A and C have been shown to be responsible for nuclear strain stiffening (25). Conducting AFM force volume mapping experiments at such large deformations in a reproducible way is technically challenging and the mechanical response can contain multiple viscoelastic moduli components (25). To resolve this challenge, we looked to our previous AFM indentation studies of HSV-1 capsids alone on a glass substrate, in which we found that probing DNA-filled C-capsids with an AFM tip can provide the mechanical response of protein capsid only without stiffness contribution from the tightly packaged intracapsid DNA, despite tens of atmospheres of DNA pressure exerted on the capsid walls (53). This is because the capsid is more rigid than the DNA, which behaves more like a fluid inside the capsid upon AFM indentation. (Note that capsids have pores and are permeable to water and ions, allowing viscoelastic deformation similar to the nucleus, which is permeable through the NPCs; Ref. 63.) Thus, to measure and separate the nuclear lamina mechanical response to AFM force volume mapping from the contribution from chromatin to the overall nucleus stiffness, nuclear lamina rigidity needs to be increased above that of chromatin. This can be achieved by chemically cross-linking the nuclear lamina shell with 2% GA. GA is a cross-linking agent that mainly cross-links proteins but not nucleic acids (39), freely crosses nuclear membranes, does not react with either DNA or RNA at room temperature (therefore, GA fixation preserves chromatin structure without inducing major artifacts; Ref. 39), and has been shown to effectively cross-link lamina structure (40). Electron microscopic localization of lamins in isolated rat liver nuclei showed that lamins are present at the nuclear periphery and are absent from more internal regions of the nucleus (40). Therefore, GA fixation of nuclei for AFM force volume mapping leads to decoupling of nuclear lamina shell mechanics from the chromatin contribution to the nucleus stiffness by inducing high lamina rigidity exceeding that of chromatin.

As described above, the lamina forms a meshwork of filaments under the nuclear membrane. The elasticity of the lamina is directly reflected by the density of the lamina meshwork. Mechanical stress exerted on the nucleus has been found to lead to remodeling of lamin A/C, resulting in change in the lamina filament multimerization and density (leading to higher

Table 1. Average Young's moduli for nuclei without capsids, nuclei with attached A-capsids, and nuclei with attached C-capsids, respectively, with and without 2% GA fixation

	Nuclei only (kPa)		Nuclei + A-capsids (kPa)		Nuclei + C-capsids (kPa)	
	Average	SE	Average	SE	Average	SE
Fixed	476.4	11.7	174.3	3.1	108.1	1.3
Unfixed	49.6	0.6	17.2	0.2	242.8	3.2

The Gaussian fit to the data in the histograms yields the average value and the SE.

or lower meshwork density or even lamina deconstruction and rupture) (7, 64, 65). While cross-linking the lamina for AFM force volume mapping of the nucleus surface will not provide a true Young's modulus value of the lamina meshwork, we are interested in capturing, with GA fixation, the change in the relative lamina stiffness (affected by lamina meshwork density) before and after herpesvirus DNA ejection into the nucleus. Thus, HSV-1 A- and C-capsids, respectively, were first incubated with nuclei to allow DNA ejection to occur from C-capsids into nuclei prior to GA fixation. After incubating nuclei and capsids in cytosol with ATP-regeneration system for 40 min at 37 °C, samples were treated with 2% GA and washed in CBB and deposited on AFM substrate for the force volume mapping experiment. By GA fixation of nuclei alone, as well as GA fixation of nuclei after they have been incubated with HSV-1 empty A-capsids and DNA-filled C-capsids, we essentially fixate lamina density before and after viral DNA ejection. As in the experiments above, force volume maps (10 × 10) were acquired at the center of each nucleus, providing Fz curves with the same acquisition parameters as in the measurements on unfixed nuclei above. Young's moduli for Fz curves in each force volume map were derived using Hertz model (8, 9). Similarly, to the observations of nuclei with capsids without GA fixation, we also observed here that some Fz curves displayed a "notch" in the deformation behavior when the AFM cantilever is placed on top of the capsid attached to the nucleus. Then, we could calculate the modulus of capsid and nucleus indentation by fitting the first Fz slope (corresponding to capsid indentation) before the notch. To calculate the second slope, associated with the indentation into the nucleus, the fit range was set ∼10 to 85% of indention depth (z) and manually adjusted to follow the contour of the second slope, which was identical to the slope in the Fz curve without the notch. However, the modulus of capsids was lower than the modulus of the nucleus, confirming that nuclear lamina rigidity is significantly increased by GA fixation. (Only the nucleus modulus was used for histogram data analysis of nucleus stiffness below.) For comparison, moduli of nuclei and capsids without fixation were essentially the same, equal to the stiffness of nucleus alone. This observation also demonstrates why AFM imaging resolution is significantly improved for capsids on nucleus surface with GA fixation.

Fig. 6*B* shows histograms for Young's moduli for all three fixated samples (force volume maps for each sample were collected on multiple nuclei and also at several locations on each nucleus). The Gaussian fit to the data in the histograms yields the average value and the SE. The measured average Young's moduli for GA fixated samples were E (nucleus without capsids) ∼476.4 ± 11.7 kPa, E (nucleus with A-capsids) ∼174.3 ± 3 kPa, and E (nucleus with C-capsids) ∼108.1 ± 1.3 kPa; see Table 1. First, comparing moduli for nuclei only, without and with GA fixation, shows a major increase in the lamina stiffness by ∼10 times (from ∼50 to ∼476 kPa). This demonstrates the effect of GA-induced lamina rigidity on lamina stiffness. This explains why AFM topographical imaging of capsids bound to the nucleus surface shown above (Fig. 4) was significantly improved with GA fixation (the nucleus surface acts as a substrate for attached capsids, and a nucleus stiffness increase by an order of magnitude stabilizes capsid AFM imaging resolution). Next, incubating empty A-capsids with nuclei (followed by GA fixation) reduced the Young's modulus by a factor of ∼3 (from 476 to 174 kPa) because of capsid interaction with NPCs, which increases nucleus wall permeability (20), leading to nucleus softening. Interestingly, the same ∼3 times stiffness reduction was also observed for unfixed nuclei incubated with A-capsids when compared to the modulus for unfixed nuclei alone. However, this stiffness decrease occurred from a much lower E-modulus value for unfixed nucleus (from 49.6 to 17.2 kPa). This nicely demonstrates that, despite GA fixation, the relative change in the stiffness of the nuclear envelope is the same as for the unfixed sample. Therefore, next we investigated the relative change in the lamina stiffness when nuclei were incubated with DNA-filled C-capsids (resulting in DNA ejection) followed by GA fixation, compared to the lamina stiffness when nuclei were incubated with empty A-capsids and fixated.

Instead of the expected increase in nucleus stiffness (observed for unfixed nuclei, where mechanical response was dominated by chromatin), we observed an ∼1.6 times stiffness decrease (from 174 to 108 kPa) compared to nuclei stiffness with docked A-capsids (Fig. 6*B* and Table 1). The observed nucleus softening suggests that the nuclear lamina meshwork became less dense (prior to GA fixation) and therefore more elastic when viral genome is ejected into the nucleus. Mechanical softening of nuclear lamina has been previously shown to provide a more robust nucleus, able to withstand strain by dissipating the mechanical stress through stretching of the lamina (7). This preserves nuclear integrity and prevents nuclear DNA damage. It can be noted that stiffness of the nucleus with docked C-capsids without GA fixation is ∼476 kPa (reflecting chromatin stiffness), while stiffness of the nucleus with docked C-capsids after GA fixation is ∼108 kPa. This illustrates that chromatin does not contribute to nucleus stiffness after GA fixation, the same way that DNA packaged in rigid HSV-1 capsids does not contribute to the capsid stiffness measured with AFM nanoindentation (45).

While increased chromatin stiffness helps to maintain nucleus integrity and morphology (25), softening of the nuclear lamina, on the other hand, helps to redistribute the mechanical stress, allowing the nucleus to restore its steady-state nuclear and chromatin architecture for long-term mechanoprotection (7). Strikingly, this occurs immediately after herpesvirus genomes are ejected into nucleus, prior to viral DNA replication, which, over time, marginalizes cellular chromatin, displacing it toward the nuclear periphery (28). Stiffer nuclei deform less upon stretching and would otherwise be subjected to increased nuclear membrane tension from viral genome ejection, which could result in nuclear rupture. Our finding demonstrates that nucleus softening induced by herpesvirus DNA ejection could provide a plausible mechanism of virus-induced mechanoadaptation of the nucleus, helping HSV-1 to establish replication compartments. Thus, we have observed the mechanoadaptation of the nucleus in the context of viral infection during early-stage internalization of viral genomes.

Conclusions

Every infected cell can produce hundreds to thousands of viruses until it is lysed (66). In the course of lytic infection, herpesviruses hijack nuclear DNA replication machinery immediately after viral capsids eject their genomes into the nucleus through the NPCs (∼30 min postinfection; Ref. 36) and exploit the nucleus for 12 to 24 h for herpesvirus genome replication and assembly of new virions. This results in dislocation and marginalization of the nuclear chromatin to the nuclear periphery by newly formed viral DNA replication compartments (28). Eventually, the nuclear membrane is ruptured, and the cell is lysed by virus-controlled mechanisms.

In this work, we discovered major mechanical transformations in both chromatin and nuclear lamina at the initial stage of herpesvirus replication, immediately after viral genomes are ejected into the nuclear space. By decoupling the mechanical responses of chromatin and nuclear lamina, we found, with AFM force volume mapping of cell-free reconstituted nuclei incubated with HSV-1 capsids, that chromatin stiffness is dramatically increased, while nuclear laminar rigidity is decreased. Given that injection of viral DNA only changes the nucleic acid content in the nucleus by <1%, a major stiffness increase in chromatin mechanics suggests a viral DNA–induced chromatin

compaction, helping to maintain nuclear morphology (as chromatin is tethered to the nuclear lamina wall) and therefore nuclear integrity. Chromatin compaction could be induced by previously observed nonrandom interactions between viral genomes and specific host chromosome regions that regulate viral transcription and compaction through interaction with histones (30). These virus–host genome interactions force reorganization and structural changes within chromosomal DNA, affecting viral replication timing and gene expression (67). The observed softening of the nuclear lamina, on the other hand, shows that stress induced by initial herpesvirus DNA accumulation under the lamina surface (36) induces increased lamina elasticity, which can be explained by lamina rearrangement resulting in lower density of the lamina meshwork. Since the lamina acts as an internal shock absorber for mechanical deformation of the nuclear membrane, the mechanism of nuclear softening has been found to provide mechanoprotection of the nuclear envelope (7). Although the number of capsids per nucleus used in this study (100 to 200) is physiologically relevant, as discussed above, it will be interesting in the future to investigate nucleus mechanics for a range of lower capsid/nucleus ratios. This would determine the minimum number of HSV-1 genomes ejected into a nucleus required to trigger the observed mechanical response. The mechanical transformations in nuclear chromatin and lamina observed in this work are not triggered by gene expression (there is no transcription and expression in an isolated nuclei system), but rather by physicochemical and biochemical interactions between viral genomes with nuclear chromatin and with lamina meshwork. Thus, we would anticipate a nuclear mechanical response to depend on the concentration of internalized HSV-1 genomes. The mechanism of nuclear mechanoadaptation is, however, only needed to prevent nucleus rupture from the mechanical stress induced by the large number of viral genomes in the nucleus during viral replication. Thus, a scenario of low capsid/nucleus ratio could be physiologically less relevant for nucleus infection mechanics.

In conclusion, both chromatin and lamina mechanical transitions caused by herpesvirus DNA ejection lead to a robust mechanical response. Since herpesvirus replication leads to mechanical stress on the nucleus and eventually its rupture (1, 29), it is plausible to suggest that this mechanoresponse is aimed at maintaining nuclear integrity and functionality required for intranuclear viral genome replication. This is an observation of mechanoadaptation in cells utilized by HSV-1. Since all herpesviruses eject their DNA into a nucleus, it is reasonable to expect similar mechanical nuclear transformations in the course of all herpesvirus infections (this is yet to be experimentally demonstrated). Furthermore, the experimental virus–host system (used in this work for AFM force volume mapping and imaging) provides an experimental platform for analysis of nuclear mechanics coupled to dynamics of viral genome replication.

Materials and Methods

Cells and Viruses. African green monkey kidney cells (Vero; ATCC CCL-81 from American Type Culture Collection) were cultured at 37 °C in 5% CO_2 in Dulbecco's modified Eagle's medium (DMEM; Life Technologies) supplemented with 10% fetal bovine serum (Gibco), 2 mM L-glutamine (Life Technologies), and antibiotics (100 U/mL penicillin and 100 μg/mL streptomycin; Life Technologies). The KOS (Kendall O. Smith) strain of HSV-1 was used as the wild-type strain. The K26GFP HSV-1 recombinant virus (gift from Dr. Prashant Desai), which carries a GFP tag on the capsid protein VP16, was used in fluorescence studies. All viruses were amplified on Vero cells, and titers were determined on Vero cells by plaque assay. Viral plaque assays were carried out as follows: Viral stocks were serially diluted in DMEM. Aliquots were plated on six-well trays of Vero cells for 1 h at 37 °C. The inoculum was then replaced with 40% (vol/vol) carboxymethylcellulose in DMEM media. HSV-1 plaque assays were incubated for 3 to 4 d. The monolayers were stained for 1 h with crystal violet stain (Sigma-Aldrich). After removal of the stain, the trays were rinsed with water and dried, and plaques were counted.

HSV-1 Nuclear Capsid Isolation. Vero cells were grown to confluence and infected with HSV-1 KOS strain at an MOI of 5 PFU/cell for 20 h at 37 °C. Cells were scraped into solution and centrifuged at 3,500 revolutions per minute (rpm) for 10 min in a JLA-16.250 rotor. The cell pellets were resuspended in phosphate-buffered saline (PBS) (1.37 M NaCl, 27 mM KCl, 43 mM $Na_2HPO_4{\cdot}7H_2O$, 14 mM KH_2PO_4), pooled, and again centrifuged at 3,500 rpm for 10 min. This washed cell pellet was resuspended in 20 mM Tris buffer (pH 7.5) with protease inhibitor mixture (Complete; Roche) and incubated on ice for 20 min to swell the cells. The swollen cells were lysed by addition of 1.25% (vol/vol) Triton X–100 (Alfa Aesar) for 30 min on ice. Samples were centrifuged at 2000 rpm for 10 min, and the resulting nuclei pellet was resuspended in a small volume of TNE (10 mM Tris, 0.5 M NaCl, 1 mM ethylenediaminetetraacetic acid) buffer with protease inhibitor mixture. Nuclei were disrupted by sonication for 30 seconds (in 10-s intervals, iced between rounds), and large debris was cleared by brief centrifugation (maximum speed for 30 s). $MgCl_2$ and DNase I were added to the supernatant to 20 mM and 100 μg/mL, respectively, and the sample was incubated at room temperature for 20 min. The supernatant was then centrifuged at 11,750 × *g* for 90 s to pellet large debris and further cleaned of small debris by underlaying with a 3 mL cushion of 35% sucrose-TNE and centrifuging at 23,000 rpm for 1 h. The capsid-rich pellet was resuspended in TNE + protease inhibitor mixture, then loaded onto a 20 to 50% (wt/wt) TNE sucrose gradient and centrifuged at 24,000 rpm in a SW41 rotor for 1 h. The A-, B-, and C-capsid bands were extracted by side puncture, diluted at least 3× in TNE buffer and finally centrifuged at 24,000 rpm for 1 h to pellet the capsids. Capsids were gently resuspended in TNE and stored at 4 °C. The purification steps for mutant viruses were the same as described for the KOS strain (68).

Rat Liver Nuclei Isolation and Cytosol Preparation. Nuclei from rat liver cells were isolated as adapted from previously described protocol (11). The intactness of nuclei was confirmed by light microscopy, EM, and fluorescence microscopy by staining the nuclei with DAPI and by their ability to exclude fluorescently tagged (fluorescein isothiocyanate) 70-kDa dextran. The cytosol was separately prepared using BHK-21 cells.

Reconstituted Capsid–Nuclei System. An in vitro viral HSV-1 DNA translocation system was built in which the HSV-1 genome was released into the nucleoplasm in a homogenate solution mimicking the cytoplasm environment; see details in previously described protocol in Ref. 11. In a typical system, rat liver cell nuclei were incubated with C-capsids (HSV-1 or GFP-labeled HSV-1), containing 1) cytosol, 2) bovine serum albumin, and 3) ATP-regeneration system (see details in Ref. 11). The system was incubated at 37 °C for 40 min sufficient for capsid binding to nuclei. For inhibition studies, WGA was preincubated with the nuclei prior to addition of C-capsids (10). We also separately confirmed that NPCs maintain full transport functionality in the reconstituted nuclei system (verified with a fluorescently labeled nuclear localization signal; Refs. 10, 69).

AFM Sample Preparation. Prior to AFM analysis, isolated rat liver cell nuclei were first reconstituted in a cell cytosol solution with added ATP-regeneration system and then incubated for 40 min at 37 °C with purified HSV-1 DNA–filled capsids. Both cellular components are required for effective capsid binding to NPCs and opening of the NPC channel for viral DNA translocation (11, 70), but the presence of these components does not provide an active mechanism for pulling the viral genome across the NPC (20, 71, 72), which is instead driven by capsid DNA pressure (10). After binding of capsids to nuclei in cytosol reconstituted with ATP-regeneration system, the samples were washed with CBB [20 mM Hepes-KOH (pH 7.3), 80 mM potassium acetate, 2 mM dithiothreitol, 1 mM ethylene glycol-bis(β-aminoethyl ether)-N,N,N′,N′-tetraacetic acid, 2 mM magnesium acetate, 1 mM phenylmethylsulfonyl fluoride, and 1x cOmplete Protease Inhibitor Cocktail (Roche)] and the sample was deposited on a glass coverslip and incubated in a covered petri dish for 30 min to allow the nuclei to adhere to the hydrophobic glass substrate. The details of substrate and sample preparations can be found elsewhere (68, 73, 74). For fixed nuclei samples, after incubation of capsids with nuclei in cytosol reconstituted with ATP-regeneration system, the samples were washed 2× with CBB (by centrifugation at 3500 rpm for 10 min at 4 °C), then fixed with 2% GA (the pellet was resuspended in 2% GA in PBS) in PBS from 1 to 3 h. After fixation, the nuclei–capsid samples were washed 2× in CBB, resuspended, and placed on the hydrophobically modified glass coverslips.

Fluorescence Microscopy. For fluorescence imaging of the reconstituted capsid–nuclei system, GFP-labeled HSV-1 C-capsids were used. After incubation of capsids with the nuclei as described above, the buffer system containing purified GFP-labeled C-capsids and nuclei were loaded onto coverslips (Mab-Tek). The nuclei were stained with DAPI for 5 min before imaging.

Overlay of the confocal 488 (for GFP emitted signal) and 358 (for DAPI emitted signal) channels show the localization of viral capsids onto the nucleus. Images were captured with a Nikon A1R laser-scanning confocal microscope. For inhibition studies with WGA, the nuclei were preincubated with 0.5 mg of WGA/mL for 20 min on ice before addition of GFP-labeled HSV-1 C-capsids.

Quantification of Capsids Bound per Nucleus. For quantification of capsids bound per nucleus, 3D stacks of nuclei with capsids were collected with Nikon A1R laser-scanning confocal microscope using oil immersion Apochromat total internal reflection fluorescence 100× (NA 1.49) differential interference contrast objective. The following image processing sequence was used for analysis: 1) separation of blue and green channels and application of a median filter to increase the signal/noise ratio; 2) Z-projection of the image stacks using blue channel to enhance the definition of each nucleus to locate the region of interest and define the periphery of the nucleus used to allocate capsids; 3) Z-projection of the 3D stacks from the green channel to highlight the location of the most brilliant nonpixels (nonoverlapping from each confocal slice) used to quantify the number of capsids attached around the nucleus surface. Z-projection shows both channels and exhibits the projection of all capsids on a nucleus; and 4) application of a threshold to the green channel converting it to a binary image used for capsid quantification. Some nuclei had visible capsid aggregates, which were converted to a number of individual capsids using number of pixels corresponding to a single capsid at the nuclear membrane surface. Number of pixels for an individual capsid was separately determined using green channel capsid brightness profile relative to the background from at least 50 capsids. This brightness profile shows a Gaussian distribution, in which width is associated with the spot diameter used to calculate capsid area based on circular object as a first approximation.

Super-Resolution Structured Illumination Microscopy. After incubation of nuclei with GFP-labeled C-capsids, the complete binding mixture was loaded onto chamber slides (Mab-Tek), and the samples were immediately imaged for GFP and DAPI by using 405-nm and 488-nm excitation wavelengths with a Zeiss Elyra S1 microscope with a 64× oil immersion lens. The images were captured on a scientific complementary metal-oxide-semiconductor Pioneers in Cameras and Optoelectronics Edge camera. The images were processed using the Structured Illumination module of the Zeiss (Zen 2011) software to obtain the super-resolved images of GFP capsids bound to nuclei. The spatial resolution of the instrument is 120 nm. To generate 3D reconstructions, image stacks (1 μm) were acquired in Frame Fast mode with a z-step of 110 nm and 120 raw images per plane. Raw data were then computationally reconstructed using the Zen software to obtain a super-resolution 3D image stack. The Fiji-ImageJ software was used to generate the histogram of the cross-section profile for the GFP-labeled C-capsid signal.

Atomic Force Microscopy. All AFM measurements were acquired on the Cypher ES atomic force microscope (Oxford Instruments Asylum Research) using Olympus AC40TS (Biolever mini) silicon nitride cantilevers (nominal spring constant is 0.1 N/m). The actual cantilever sensitivity and spring constant of each cantilever were determined using the GetReal calibration routine built into the Asylum MFP3D software. Target nuclei were located optically, and the cantilever was precisely placed above the center of each nucleus before the automated tip approach. High-resolution images of nuclei with bound capsids were acquired in FFM mode at a pixel density of 256 × 256, force setpoint of 2 nN, and a tapping frequency of 500 Hz. Using AFM to resolve high-resolution structures of viral capsids on the nucleus surface requires control of the tip-sample interaction at low force. We show here that this is achieved using FFM mode. With FFM, topographical and nanomechanical data (based on Fz curves) can be acquired at higher frequencies, overcoming the slow acquisition times typical of standard force volume maps and allowing for the visualization of high-resolution structural details because of higher pixel density. Unlike Tapping Mode, in FFM the AFM tip is oscillated at subresonance frequency with fewer taps and is fully retracted from the sample surface before moving to the next point, thus preventing lateral movement and sample deformation and resulting in higher imaging resolution. FFM provides controlled, low-force indentation at every point, in the range of piconewtons. This is in contrast to Tapping Mode, in which force is difficult to control because of instability of the force feedback, which can lead to large transient forces and potential sample damage) (51). In general, using soft cantilevers (<0.2 N/m) and low-force setpoints (subnanonewtons) with FFM is proving to be a preferred technique to image soft, poorly attached, or overall difficult to image samples.

For nanomechanical measurements, a 10 × 10 force volume map (also called Force Map on Asylum AFM instruments) was acquired over a 200 nm × 200 nm area at the center of each nuclei, where the surface is typically the flattest. Acquisition parameters were 300 nm/s for AFM tip velocity (we determined the equilibrium indentation rate below which nucleus modulus does not change; see *SI Appendix*, Fig. 1), 1 μm force distance (the AFM tip pull-off distance for the Fz curve needs to be far enough from the nucleus surface before moving the tip to the next position, to avoid damage to the sample), and 2 to 12 nN for force trigger (during a force curve, the AFM tip indents the sample until a trigger force threshold is reached, after which the tip is withdrawn until it loses contact with the sample). The force trigger was adjusted to achieve ∼300 nm of sample indentation. To ensure that the nucleus does not roll on the glass substrate surface during AFM indentation, lateral force was also recorded, showing no lateral drag on the cantilever tip. Several force maps were captured for each sample condition. Young's modulus of the nuclei was calculated by applying the Hertz contact mechanics model for a cone indenter to each force curve. Moduli for each force volume map was plotted in a histogram in which average moduli were calculated.

Data Availability. All study data are included in the article and/or *SI Appendix*.

ACKNOWLEDGMENTS. We greatly acknowledge Efthymios Tsimtsirakis, José Ramon Villanueva, and Alberto Brandariz for technical assistance with sample preparation and image analysis. We thank Chris Boutell, Nancy Sawtell, and Greg Smith for fruitful discussions in the course of review of this work. This work was supported by the Swedish Research Council grants (VR) 349-2014-3962 and 2019-05192 (all to A.E.) and Mats Paulsson Foundation to A.E.

1. J. M. Bigalke, E. E. Heldwein, Nuclear exodus: Herpesviruses lead the way. *Annu. Rev. Virol.* **3**, 387–409 (2016).
2. M. A. Maroui *et al.*, Latency entry of herpes simplex virus 1 is determined by the interaction of its genome with the nuclear environment. *PLoS Pathog.* **12**, e1005834 (2016).
3. N. Jourdan *et al.*, Live-cell imaging reveals multiple interactions between Epstein-Barr virus nuclear antigen 1 and cellular chromatin during interphase and mitosis. *J. Virol.* **86**, 5314–5329 (2012).
4. N. Koushki *et al.*, Lamin A redistribution mediated by nuclear deformation determines dynamic localization of YAP. bioRxiv [Preprint] (2020). doi.org/10.1101/2020.03.19.998708.
5. E. S. Scott, P. O'Hare, Fate of the inner nuclear membrane protein lamin B receptor and nuclear lamins in herpes simplex virus type 1 infection. *J. Virol.* **75**, 8818–8830 (2001).
6. G. L. Cano-Monreal, K. M. Wylie, F. Cao, J. E. Tavis, L. A. Morrison, Herpes simplex virus 2 UL13 protein kinase disrupts nuclear lamins. *Virology* **392**, 137–147 (2009).
7. M. M. Nava *et al.*, Heterochromatin-driven nuclear softening protects the genome against mechanical stress-induced damage. *Cell* **181**, 800–817.e22 (2020).
8. D. C. Lin, E. K. Dimitriadis, F. Horkay, Robust strategies for automated AFM force curve analysis-II: Adhesion-influenced indentation of soft, elastic materials. *J. Biomech. Eng.* **129**, 904–912 (2007).
9. D. C. Lin, E. K. Dimitriadis, F. Horkay, Robust strategies for automated AFM force curve analysis–I. Non-adhesive indentation of soft, inhomogeneous materials. *J. Biomech. Eng.* **129**, 430–440 (2007).
10. A. Brandariz-Nuñez, T. Liu, T. Du, A. Evilevitch, Pressure-driven release of viral genome into a host nucleus is a mechanism leading to herpes infection. *eLife* **8**, e47212 (2019).
11. P. M. Ojala, B. Sodeik, M. W. Ebersold, U. Kutay, A. Helenius, Herpes simplex virus type 1 entry into host cells: Reconstitution of capsid binding and uncoating at the nuclear pore complex in vitro. *Mol. Cell. Biol.* **20**, 4922–4931 (2000).
12. D. Dünn-Kittenplon *et al.*, The portal vertex of KSHV promotes docking of capsids at the nuclear pores. *Viruses* **13**, e47212 (2021).
13. M. Krause, J. Te Riet, K. Wolf, Probing the compressibility of tumor cell nuclei by combined atomic force-confocal microscopy. *Phys. Biol.* **10**, 065002 (2013).
14. A. J. Zuckerman, Fields Virology, 3rd edn. (two vol. set). *FEBS Lett.* **388**, 88 (1996).
15. T. Alandijany *et al.*, Distinct temporal roles for the promyelocytic leukaemia (PML) protein in the sequential regulation of intracellular host immunity to HSV-1 infection. *PLoS Pathog.* **14**, e1006769 (2018).
16. M. M. Shipley *et al.*, Genome-wide surveillance of genital herpes simplex virus type 1 from multiple anatomic sites over time. *J. Infect. Dis.* **218**, 595–605 (2018).
17. N. M. Sawtell, Comprehensive quantification of herpes simplex virus latency at the single-cell level. *J. Virol.* **71**, 5423–5431 (1997).
18. N. M. Sawtell, D. K. Poon, C. S. Tansky, R. L. Thompson, The latent herpes simplex virus type 1 genome copy number in individual neurons is virus strain specific and correlates with reactivation. *J. Virol.* **72**, 5343–5350 (1998).
19. R. L. Thompson, N. M. Sawtell, Replication of herpes simplex virus type 1 within trigeminal ganglia is required for high frequency but not high viral genome copy number latency. *J. Virol.* **74**, 965–974 (2000).
20. T. Hennig, P. O'Hare, Viruses and the nuclear envelope. *Curr. Opin. Cell Biol.* **34**, 113–121 (2015).
21. P. M. Lieberman, Chromatin organization and virus gene expression. *J. Cell. Physiol.* **216**, 295–302 (2008).

22. T. C. Mettenleiter, Breaching the barrier-the nuclear envelope in virus infection. *J. Mol. Biol.* **428** (10 Pt A), 1949–1961 (2016).
23. Y. Gruenbaum, R. Foisner, Lamins: Nuclear intermediate filament proteins with fundamental functions in nuclear mechanics and genome regulation. *Annu. Rev. Biochem.* **84**, 131–164 (2015).
24. A. Buchwalter, J. M. Kaneshiro, M. W. Hetzer, Coaching from the sidelines: The nuclear periphery in genome regulation. *Nat. Rev. Genet.* **20**, 39–50 (2019).
25. A. D. Stephens, E. J. Banigan, S. A. Adam, R. D. Goldman, J. F. Marko, Chromatin and lamin A determine two different mechanical response regimes of the cell nucleus. *Mol. Biol. Cell* **28**, 1984–1996 (2017).
26. A. Vaziri, H. Lee, M. Mofrad, Deformation of the cell nucleus under indentation: Mechanics and mechanisms. *J. Mater. Res.* **21**, 2126–2135 (2006).
27. E. Latorre *et al.*, Active superelasticity in three-dimensional epithelia of controlled shape. *Nature* **563**, 203–208 (2018).
28. M. Simpson-Holley, R. C. Colgrove, G. Nalepa, J. W. Harper, D. M. Knipe, Identification and functional evaluation of cellular and viral factors involved in the alteration of nuclear architecture during herpes simplex virus 1 infection. *J. Virol.* **79**, 12840–12851 (2005).
29. J. Cibulka, M. Fraiberk, J. Forstova, Nuclear actin and lamins in viral infections. *Viruses* **4**, 325–347 (2012).
30. H. Li *et al.*, Specific virus-host genome interactions revealed by tethered chromosome conformation capture. *bioRxiv* [Preprint] (2017). https://doi.org/10.1101/142604.
31. A. D. Stephens, Chromatin rigidity provides mechanical and genome protection. *Mutat. Res.* **821**, 111712 (2020).
32. E. T. Sieradzki, J. C. Ignacio-Espinoza, D. M. Needham, E. B. Fichot, J. A. Fuhrman, Dynamic marine viral infections and major contribution to photosynthetic processes shown by spatiotemporal picoplankton metatranscriptomes. *Nat. Commun.* **10**, 1169 (2019).
33. D. W. Bauer, J. B. Huffman, F. L. Homa, A. Evilevitch, Herpes virus genome, the pressure is on. *J. Am. Chem. Soc.* **135**, 11216–11221 (2013).
34. B. Sodeik, M. W. Ebersold, A. Helenius, Microtubule-mediated transport of incoming herpes simplex virus 1 capsids to the nucleus. *J. Cell Biol.* **136**, 1007–1021 (1997).
35. G. A. Smith, Navigating the cytoplasm: Delivery of the alphaherpesvirus genome to the nucleus. *Curr. Issues Mol. Biol.* **41**, 171–220 (2021).
36. E. Sekine, N. Schmidt, D. Gaboriau, P. O'Hare, Spatiotemporal dynamics of HSV genome nuclear entry and compaction state transitions using bioorthogonal chemistry and super-resolution microscopy. *PLoS Pathog.* **13**, e1006721 (2017).
37. H. J. G. van de Werken *et al.*, "Chapter Four - 4C Technology: Protocols and Data Analysis" in *Methods in Enzymology*, C. Wu, C. D. Allis, Eds. (Academic Press, 2012), vol. **513**, pp. 89–112.
38. C. Guilluy *et al.*, Isolated nuclei adapt to force and reveal a mechanotransduction pathway in the nucleus. *Nat. Cell Biol.* **16**, 376–381 (2014).
39. A. McKenzie, Glutaraldehyde: A review of its fixative effects on nucleic acids, proteins, lipids, and carbohydrates. *OSF* [Preprint] (2019). doi.org/10.31219/osf.io/8zd4e.
40. T. Senda, A. Iizuka-Kogo, A. Shimomura, Visualization of the nuclear lamina in mouse anterior pituitary cells and immunocytochemical detection of lamin A/C by quick-freeze freeze-substitution electron microscopy. *J. Histochem. Cytochem.* **53**, 497–507 (2005).
41. G. G. Maul, L. Deaven, Quantitative determination of nuclear pore complexes in cycling cells with differing DNA content. *J. Cell Biol.* **73**, 748–760 (1977).
42. A. K. Sheaffer *et al.*, Herpes simplex virus DNA cleavage and packaging proteins associate with the procapsid prior to its maturation. *J. Virol.* **75**, 687–698 (2001).
43. B. L. Trus *et al.*, The herpes simplex virus procapsid: Structure, conformational changes upon maturation, and roles of the triplex proteins VP19c and VP23 in assembly. *J. Mol. Biol.* **263**, 447–462 (1996).
44. E. Medina, E. Nakatani, S. Kruse, C. E. Catalano, Thermodynamic characterization of viral procapsid expansion into a functional capsid shell. *J. Mol. Biol.* **418**, 167–180 (2012).
45. U. Sae-Ueng *et al.*, Major capsid reinforcement by a minor protein in herpesviruses and phage. *Nucleic Acids Res.* **42**, 9096–9107 (2014).
46. D. R. Finlay, D. D. Newmeyer, T. M. Price, D. J. Forbes, Inhibition of in vitro nuclear transport by a lectin that binds to nuclear pores. *J. Cell Biol.* **104**, 189–200 (1987).
47. U. F. Greber *et al.*, The role of the nuclear pore complex in adenovirus DNA entry. *EMBO J.* **16**, 5998–6007 (1997).
48. S. J. Flint, V. R. Racaniello, G. F. Rall, T. Hatziioannou, A. M. Skalka, *Principles of Virology* (Wiley & American Society for Microbiology, Hoboken, NJ, 2020), p. 1 online resource.
49. A. Brandariz-Nuñez, S. J. Robinson, A. Evilevitch, Pressurized DNA state inside herpes capsids-A novel antiviral target. *PLoS Pathog.* **16**, e1008604 (2020).
50. A. Meyring-Wösten, W. Hafezi, J. Kühn, I. Liashkovich, V. Shahin, Nano-visualization of viral DNA breaching the nucleocytoplasmic barrier. *J. Control. Release* **173**, 96–101 (2014).
51. H. Schillers, I. Medalsy, S. Hu, A. L. Slade, J. E. Shaw, PeakForce Tapping resolves individual microvilli on living cells. *J. Mol. Recognit.* **29**, 95–101 (2016).
52. A. Weber, J. Iturri, R. Benitez, J. L. Toca-Herrera, Measuring biomaterials mechanics with atomic force microscopy. 1. Influence of the loading rate and applied force (pyramidal tips). *Microsc. Res. Tech.* **82**, 1392–1400 (2019).
53. U. Sae-Ueng *et al.*, Solid-to-fluid DNA transition inside HSV-1 capsid close to the temperature of infection. *Nat. Chem. Biol.* **10**, 861–867 (2014).
54. M. J. Rosenbluth, W. A. Lam, D. A. Fletcher, Force microscopy of nonadherent cells: A comparison of leukemia cell deformability. *Biophys. J.* **90**, 2994–3003 (2006).
55. J. Rother, H. Nöding, I. Mey, A. Janshoff, Atomic force microscopy-based microrheology reveals significant differences in the viscoelastic response between malign and benign cell lines. *Open Biol.* **4**, 140046 (2014).
56. W. W. Newcomb, D. R. Thomsen, F. L. Homa, J. C. Brown, Assembly of the herpes simplex virus capsid: Identification of soluble scaffold-portal complexes and their role in formation of portal-containing capsids. *J. Virol.* **77**, 9862–9871 (2003).
57. C. M. Hobson *et al.*, Correlating nuclear morphology and external force with combined atomic force microscopy and light sheet imaging separates roles of chromatin and lamin A/C in nuclear mechanics. *Mol. Biol. Cell* **31**, 1788–1801 (2020).
58. M. Hernando-Pérez, C. Zeng, M. C. Miguel, B. Dragnea, Intermittency of deformation and the elastic limit of an icosahedral virus under compression. *ACS Nano* **13**, 7842–7849 (2019).
59. G. Kaushik, A. Fuhrmann, A. Cammarato, A. J. Engler, In situ mechanical analysis of myofibrillar perturbation and aging on soft, bilayered Drosophila myocardium. *Biophys. J.* **101**, 2629–2637 (2011).
60. J. B. Huffman *et al.*, The C terminus of the herpes simplex virus UL25 protein is required for release of viral genomes from capsids bound to nuclear pores. *J. Virol.* **91**, e00641-17 (2017).
61. D. Pasdeloup, D. Blondel, A. L. Isidro, F. J. Rixon, Herpesvirus capsid association with the nuclear pore complex and viral DNA release involve the nucleoporin CAN/Nup214 and the capsid protein pUL25. *J. Virol.* **83**, 6610–6623 (2009).
62. A. D. Stephens *et al.*, Chromatin histone modifications and rigidity affect nuclear morphology independent of lamins. *Mol. Biol. Cell* **29**, 220–233 (2018).
63. R. Kapon *et al.*, Permeating the nuclear pore complex. *Nucleus* **1**, 475–480 (2010).
64. J. L. Broers *et al.*, Decreased mechanical stiffness in LMNA-/- cells is caused by defective nucleo-cytoskeletal integrity: Implications for the development of laminopathies. *Hum. Mol. Genet.* **13**, 2567–2580 (2004).
65. J. Lammerding *et al.*, Lamin A/C deficiency causes defective nuclear mechanics and mechanotransduction. *J. Clin. Invest.* **113**, 370–378 (2004).
66. C. Zimmer, A *P*lanet of *V*iruses (The University of Chicago Press, Chicago; London, ed. 3, 2021).
67. R. Ferrari *et al.*, Reorganization of the host epigenome by a viral oncogene. *Genome Res.* **22**, 1212–1221 (2012).
68. K. G. Freeman, J. B. Huffman, F. L. Homa, A. Evilevitch, UL25 capsid binding facilitates mechanical maturation of the Herpesvirus capsid and allows retention of pressurized DNA. *J. Virol.* **95**, e0075521 (2021).
69. Y. Miyamoto *et al.*, Importin alpha can migrate into the nucleus in an importin beta- and Ran-independent manner. *EMBO J.* **21**, 5833–5842 (2002).
70. F. Anderson *et al.*, Targeting of viral capsids to nuclear pores in a cell-free reconstitution system. *Traffic* **15**, 1266–1281 (2014).
71. N. Fay, N. Panté, Nuclear entry of DNA viruses. *Front. Microbiol.* **6**, 467 (2015).
72. I. Liashkovich, W. Hafezi, J. M. Kühn, H. Oberleithner, V. Shahin, Nuclear delivery mechanism of herpes simplex virus type 1 genome. *J. Mol. Recognit.* **24**, 414–421 (2011).
73. I. Ivanovska, G. Wuite, B. Jönsson, A. Evilevitch, Internal DNA pressure modifies stability of WT phage. *Proc. Natl. Acad. Sci. U.S.A.* **104**, 9603–9608 (2007).
74. I. L. Ivanovska *et al.*, Bacteriophage capsids: Tough nanoshells with complex elastic properties. *Proc. Natl. Acad. Sci. U.S.A.* **101**, 7600–7605 (2004).